Astaxanthin induces NADPH oxidase activation and receptor-interacting protein kinase 1-mediated necroptosis in gastric cancer AGS cells

SORI KIM, HANBIT LEE, JOO WEON LIM and HYEYOUNG KIM

Department of Food and Nutrition, Brain Korea 21 FOUR Project, College of Human Ecology, Yonsei University, Seoul 03722, Republic of Korea

Received July 21, 2021; Accepted September 22, 2021

DOI: 10.3892/mmr.2021.12477

Abstract. Astaxanthin (ASX), a red-colored xanthophyll carotenoid, functions as an antioxidant or pro-oxidant. ASX displays anticancer effects by reducing or increasing oxidative stress. Reactive oxygen species (ROS) promote cancer cell death by necroptosis mediated by receptor-interacting protein kinase 1 (RIP1) and RIP3. NADPH oxidase is a major source of ROS that may promote necroptosis in some cancer cells. The present study aimed to investigate whether ASX induces necroptosis by increasing NADPH oxidase activity and ROS levels in gastric cancer AGS cells. AGS cells were treated with ASX with or without ML171 (NADPH oxidase 1 specific inhibitor), N-acetyl cysteine (NAC; antioxidant), z-VAD (pan-caspase inhibitor) or Necrostatin-1 (Nec-1; a specific inhibitor of RIP1). As a result, ASX increased NADPH oxidase activity, ROS levels and cell death, and these effects were suppressed by ML171 and NAC. Furthermore, ASX induced RIP1 and RIP3 activation, ultimately inducing mixed lineage kinase domain-like protein (MLKL) activation, lactate dehydrogenase (LDH) release and cell death. Moreover, the ASX-induced decrease in cell viability was reversed by Nec-1 treatment and RIP1 siRNA transfection, but not by z-VAD. ASX did not increase the ratio of apoptotic Bax/anti-apoptotic Bcl-2, the number of Annexin V-positive cells, or caspase-9 activation, which are apoptosis indices. In conclusion, ASX induced necroptotic cell death by increasing NADPH oxidase activity, ROS levels, LDH release and the number of propidium iodide-positive cells, as well as activating necroptosis-regulating proteins, RIP1/RIP3/MLKL, in gastric cancer AGS cells. The results of this study demonstrated the necroptotic effect of ASX on gastric cancer AGS cells, which required NADPH oxidase activation and RIP1/RIP3/MLKL signaling *in vitro*.

Correspondence to: Professor Hyeyoung Kim, Department of Food and Nutrition, Brain Korea 21 FOUR Project, College of Human Ecology, Yonsei University, 50 Yonsei-ro, Seodaemun-gu, Seoul 03722, Republic of Korea
E-mail: kim626@yonsei.ac.kr

Key words: astaxanthin, gastric cancer cells, NADPH oxidase, receptor interacting protein kinase 1, reactive oxygen species

Introduction

Astaxanthin (ASX) is a naturally occurring red-colored oxygenated carotenoid that is present in microalgae, salmon, trout and shrimp (1). Owing to its structure, which consists of a long backbone and hydroxyl and keto moieties at each polar end, ASX has especially powerful antioxidant capacity compared with other carotenoids (2). ASX has no adverse effects (3), and there is evidence of a reduction in biomarkers of oxidative stress and inflammation with ASX administration (4).

ASX has been shown to inhibit cancer cell proliferation by reducing or increasing oxidative stress (5-10). It has been reported that ASX (100-300 μM) decreases NF-κB and Wnt/β-catenin levels, thereby inhibiting hepatic cancer cell proliferation (5). ASX (50 and 100 μM) has been shown to inhibit the proliferation of Kato-III and SNU cells by suppressing cell cycle progression (6). With respect to antioxidant activity in anticancer mechanisms, ASX (50-150 μM) is known to induce apoptosis by increasing the expression levels of apoptotic Bax and caspase-3, but decreasing anti-apoptotic Bcl-2 levels in colorectal cancer LS-180 cells (7). Kochi *et al* (8) showed that ASX treatment inhibited azoxymethane-induced neoplastic lesions in the colonic mucosa of mice. ASX administration reduced serum levels of hydroperoxides, an oxidative stress marker, but increased the colonic mucosal levels of antioxidant enzymes (superoxide dismutase, catalase and glutathione peroxidase). These studies suggest that ASX reduces oxidative stress-mediated cancer cell growth.

By contrast, recent studies have reported the pro-oxidant effects of ASX on cancer cells. In one study, ASX (10, 25, 50 and 100 $\mu g \cdot ml^{-1}$) induced cell death in a dose- and time-dependent manner (24, 48 and 72 h) in human non-small cell lung cancer A549 cells (9). ASX (50 $\mu g \cdot ml^{-1}$) increased reactive oxygen species (ROS) levels (195% of untreated cells) after 4 h of culture in A549 cells (9). In breast cancer MCF-7 cells, ASX (20, 30, 40 and 50 μM) decreased cell viability in a dose- and time-dependent manner (24, 28 and 72 h culture). Cells

cultured for 48 h with ASX (20 μM) increased ROS levels to 153% of that of the untreated cells (10). Therefore, ASX may exhibit its anticancer effect through the production of ROS and ROS-mediated death signaling pathways.

Necroptosis is programmed necrosis, which is regulated by necroptotic regulators, such as receptor-interacting protein kinase 1 (RIP1), RIP3 and mixed lineage kinase domain-like protein (MLKL) (11,12). Upon stimulation, including the activation of Toll-like receptors (13), T cell receptors (14) and the TNF receptor superfamily (15), the serine/threonine kinase activity of RIP1 and RIP3 increases, and consecutive phosphorylation of RIP1 and RIP3 forms a RIP1-RIP3 heterodimeric scaffold complex. However, necrosis represents a form of non-programmed cell death. Therefore, necrosis is not regulated by necroptotic regulators, such as RIP1, RIP3 and MLKL (16).

After formation of the RIP1-RIP3 heterodimeric scaffold complex, free RIP3 is recruited and auto-phosphorylated. This allows the recruitment of MLKL to form the necrosome (17,18). Phosphorylated MLKL translocates to the plasma membrane and oligomerizes into complexes, leading to plasma membrane rupture, thereby acting as an executioner of necroptosis (13). Dysregulation of necroptotic proteins results in cancer development (19). RIP3 is lower in breast and colorectal cancer cells than in healthy cells, and low RIP3 expression levels are associated with poor survival in patients with cancer (12,20). MLKL levels are lower in gastric cancer tissues than in normal tissues (21).

ROS activate RIP1 autophosphorylation and contribute to RIP3 recruitment into the necrosome (22,23). NADPH oxidase produces large amounts of ROS upon exposure to various stimuli (24). Thus, NADPH oxidase activation may mediate necroptosis by activating RIP1-RIP3-MLKL signaling in cancer cells.

The present study aimed to determine whether ASX induces necroptosis by activating necroptotic proteins (RIP1, RIP3 and MLKL) and cell death [by determining lactate dehydrogenase (LDH) release, propidium iodide (PI)-positive cells and cell viability] in gastric cancer AGS cells. In addition, to investigate whether ASX-induced necroptosis is induced by NADPH oxidase activation and increased ROS levels, the cells were treated with the NADPH oxidase inhibitor ML171 or antioxidant N-acetylcysteine (NAC) prior to ASX treatment. Moreover, to assess whether ASX affects the viability of normal gastric epithelial cells, normal RGM-1 cells were treated with ASX, and cell viability and NADPH oxidase activity were measured.

Materials and methods

Materials. ASX (cat. no. SML0982), necrotatin-1 (Nec-1; the stable variant; cat. no. 5042970001), z-VAD-fmk (cat. no. 627610), ML171 (cat. no. 492002) and N-acetylcysteine (NAC; cat. no. A7250) were purchased from Sigma-Aldrich (Merck KGaA). Dichlorofluorescein diacetate (DCF-DA; cat. no. D399) was purchased from Molecular Probes (Thermo Fisher Scientific, Inc.). RPMI-1640 medium (cat. no. 31800022) was purchased from Gibco (Thermo Fisher Scientific, Inc.). MuLV reverse transcriptase (cat. no. M1705) was obtained from Promega Corporation. The protease inhibitor complex (cOmplete™; cat. no. 11697498001) was obtained from Roche Diagnostics GmbH. Antibodies against caspase-9 (cat. no. sc-81663), Bcl-2 (cat. no. sc-492), Bax (cat. no. sc-526) and actin (cat. no. sc-47778) were obtained from Santa Cruz Biotechnology, Inc. Antibodies against phosphorylated (p)-RIP1 (cat. no. 65746) and p-MLKL (cat. no. 91689) were obtained from Cell Signaling Technology, Inc. The antibody against RIP1 (cat. no. 610458) was obtained from BD Pharmingen (BD Biosciences). Antibodies against RIP3 (cat. no. ab56164), p-RIP3 (cat. no. ab209384) and MLKL (cat. no. ab183770) were obtained from Abcam. All other reagents were obtained from Sigma-Aldrich (Merck KGaA). ASX, NEC-1, z-VAD-fmk and ML171 were dissolved in dimethyl sulfoxide (DMSO). Cells incubated with DMSO alone (<0.3%) served as controls (vehicle alone).

Cell line and culture conditions. The human gastric cancer cell line AGS (ATCC CRL-1739; gastric adenocarcinoma) was purchased from the American Type Culture Collection and cultured in RPMI-1640 medium with 10% fetal bovine serum (FBS; Gibco; Thermo Fisher Scientific, Inc.), 2 mM glutamine and antibiotics (100 U•ml^{-1} penicillin and 100 μg•ml^{-1} streptomycin). The cells were cultured at 37˚C in a humidified atmosphere with 95% air and 5% CO_2.

The normal rat gastric epithelial cell line, RGM-1, was obtained from the RIKEN BioResource Center. RGM-1 cells were grown in a 1:1 mixture of Dulbecco's modified Eagle's medium (DMEM; Gibco; Thermo Fisher Scientific, Inc.) and Ham's F-12 medium (Gibco; Thermo Fisher Scientific, Inc.) supplemented with 20% newborn calf serum (Gibco; Thermo Fisher Scientific, Inc.), 100 U•ml^{-1} penicillin and 100 μg•ml^{-1} streptomycin. The cells were cultured at 37˚C in a humidified atmosphere with 95% air and 5% CO_2.

Experimental protocol. For all treatments, the cells were cultured at 37˚C. For the time-course experiment to determine ROS levels and necroptotic markers, the cells were treated with 20 μM ASX and cultured for 0.5, 1 and 2 h (for ROS levels) or 2, 4 and 6 h (for the mRNA and protein expression levels of RIP1, RIP3, MLKL, and p-RIP1, p-RIP3 and p-MLKL levels).

For the concentration-course experiment to assess ROS levels and cell viability, the cells were treated with ASX (5, 10 or 20 μM) for 2 h (for ROS determination) and 24 h (for analysis of cell viability).

For the assessment of ROS levels, NADPH oxidase activity, cell viability, LDH release and Hoechst 33342/propidium oxide (PI) double staining, the cells were pretreated with ML171 (2 μM), NAC (1 mM), Nec-1 (25 μM) or z-VAD-fmk (10 μM) for 1 h and treated with 20 μM ASX for 2 h (to measure levels of ROS and NADPH oxidase activity) or 24 h (for cell viability, LDH release and Hoechst 33342/PI double staining).

To assess the role of RIP1 in ASX-induced cell death, cells were transfected with RIP1 small interfering (si)RNA or negative control (NC) siRNA and treated with ASX (20 μM) for 24 h, and the number of viable cells was counted.

To determine the effect of ASX on caspase-9 activation, the levels of Bax and Bcl-2, and Annexin V-FITC/PI double staining, the cells were treated with 20 μM ASX for 24 h. Western blot analysis was used to determine the levels of procaspase-9 and cleaved caspase-9. Fluorescence images

of AGS cells were obtained by Annexin V-FITC/PI double staining.

To determine whether ASX induced cell death and activated NADPH oxidase in normal cells, normal rat gastric epithelial cells (RGM-1) were treated with 20 μM ASX for 2 h (to measure NADPH oxidase activity) or different concentrations (5, 10 or 20 μM) of ASX for 24 h (for cell viability).

Determination of intracellular ROS levels. 2'-7'-Dichlorofluorescin diacetate (DCFH-DA) was used to measure intracellular levels of ROS. This method is used to detect hydrogen peroxide and hydroxyl radicals (25). The cells were seeded ($6x10^4$ cells per well) in 6-well plates and incubated with 10 μM DCF-DA for 30 min. The cells were then washed and scraped into 1 ml PBS. DCF was measured (excitation/emission at 495/535 nm) using a VICTOR5 multilabel counter (PerkinElmer, Inc.). Intracellular ROS levels were expressed in terms of relative increases.

Cell viability measurement. The cells were plated in a 24-well plate ($1x10^4$ cells per well) and cultured for 24 h with or without treatment. Viable cell numbers were determined by direct counting using a hemocytometer based on a trypan blue exclusion test (0.2% trypan blue; Sigma-Aldrich; Merck KGaA). The mean number of viable cells that were not treated with ASX (untreated) was set to 100%.

Reverse transcription-quantitative PCR (RT-qPCR) analysis. Total RNA was isolated using the TRIzol® reagent (Invitrogen; Thermo Fisher Scientific, Inc.). RNA was converted to cDNA by reverse transcription using MuLV reverse transcriptase. The reaction conditions were as follows: 23˚C for 10 min, 37˚C for 60 min and 95˚C for 5 min. cDNA was used for qPCR. qPCR was conducted in triplicate using SYBR-Green Real-time PCR Master Mix (Toyobo Life Science). RIP1 primers (forward, 5'-GGCATTGAAGAAAAATTTAGGC-3' and reverse, 5'-TCACAACTGCATTTTCGTTTG-3') were used to generate a 109-bp PCR product, RIP3 primers (forward, 5'-GACTCCCGGCTTAGAAGGACT-3' and reverse, 5'-CTGCTCTTGAGCTGAGACAGG-3') were used to generate a 180-bp PCR product and MLKL primers (forward, 5'-AGAGCTCCAGTGGCCATAAA-3' and reverse, 5'-TACGCAGGATGTTGGGAGAT-3') were used to generate a 124-bp PCR product. For β-actin, the forward primer was 5'-ACCAACTGGGACGACATGGAG-3' and the reverse primer was 5'-GTGAGGATCTTCATGAGGTAGTC-3', yielding a 349-bp PCR product. cDNA was amplified by 45 cycles of denaturation at 95˚C for 30 sec, annealing at 55˚C for 30 sec and extension at 72˚C for 30 sec. During the first cycle, the 95˚C step was extended to 3 min. Amplification specificity was validated by melting curve analysis generated at the end of each PCR reaction. All genes presented a single peak in the melting curve, indicating the absence of primer-dimer formation during the reaction and specificity of the amplification. Relative changes in gene expression between untreated cells and cells treated with ASX were determined using the $2^{-\Delta\Delta Cq}$ method (26). Levels of the target transcript were normalized to β-actin endogenous control and were constantly expressed in the group.

Preparation of cell extracts. Preparation of whole-cell extracts, membrane fractions and cytosolic fractions was performed as previously described (27). Briefly, the cells were harvested by treatment with trypsin/EDTA, washed and centrifuged at 1,000 x g at 21-23˚C for 5 min. The cell pellets were resuspended in lysis buffer containing 150 mM NaCl, 1% NP-40, 0.5% sodium deoxycholate, 0.1% SDS, 25 mM Tris (pH 7.4) and protease inhibitor complex. The resulting mixture was centrifuged at 10,000 x g at 21-23˚C for 15 min. The supernatants were collected and used as whole-cell extracts. To prepare the cytosolic and membrane fractions, the supernatant was separated by centrifugation at 100,000 x g at 21-23˚C for 1 h. The membrane fraction was obtained by resuspending the pellet in lysis buffer containing 50 mM HEPES (pH 7.4), 150 mM NaCl, 1 mM EDTA and 10% glycerol. The supernatant was used as the cytosolic fraction. The protein concentration was determined using the Bradford assay.

Western blot analysis. Whole cell extracts were isolated from cells by using lysis buffer containing 150 mM NaCl, 1% NP-40, 0.5% sodium deoxycholate, 0.1% SDS, 25 mM Tris (pH 7.4) and protease inhibitor complex (Complete; Roche Diagnostics GmbH). The protein concentration was determined using the Bradford assay. Whole cell extracts were loaded onto 8-10% SDS-PAGE gels (40-60 μg protein per lane) and separated by electrophoresis under reducing conditions. Proteins were transferred onto nitrocellulose membranes via electroblotting. The membranes were blocked using 3% non-fat dry milk in Tris-buffered saline and 0.2% Tween-20 (TBST) for 1 h at room temperature. The membrane was incubated with antibodies against caspase-9 (1:1,000), actin (1:4,000), RIP1 (1:1,000), p-RIP1 (1:1,000), RIP3 (1:1,500), p-RIP3 (1:1,000), MLKL (1:1,500) and p-MLKL (1:1,000) in TBST solution containing 3% dry milk overnight at 4˚C. After washing with TBST, the membrane was incubated with horseradish peroxidase-conjugated anti-mouse (1:3,000; cat. no. sc-2005; Santa Cruz Biotechnology, Inc.) or anti-rabbit (1:4,000; cat. no. sc-2005; Santa Cruz Biotechnology, Inc.) secondary antibodies in TBST solution containing 3% dry milk and anti-rabbit) for 2 h at room temperature. The proteins were visualized by exposure to X-ray film by using an enhanced chemiluminescence (ECL) detection system (cat. no. sc-2048; Santa Cruz Biotechnology, Inc.). Actin was used as the loading control. ImageJ software version 1.52a (National Institutes of Health) was used for densitometry analysis of western blots.

Measurement of NADPH oxidase activity. A luciferase assay was used to measure NADPH oxidase activity in the membrane and cytosolic fractions (28). The assay was performed in 50 mM Tris-MES buffer (pH 7.0) containing 2 mM KCN, 10 μM lucigenin and 100 μM NADPH. The reaction was initiated by the addition of 10 μg membrane-extract protein. Photon emission was measured using a microplate reader (Molecular Devices, LLC). For negative control experiments, cytosolic fraction protein was used instead of the membrane-fraction protein.

PI and Hoechst 33342 double staining. PI is permeable to necrotic cells and is visible as red fluorescence in nuclear DNA (29). Hoechst staining is a cell-permeable nuclear counterstain that emits blue fluorescence when combined with double-stranded DNA (29). Hoechst dyes are very sensitive to DNA conformation and chromatin status in cells and

are, therefore, used to detect nuclear damage, such as distinguishing condensed pycnotic nuclei in apoptotic cells. PI and Hoechst 33342 double staining was used to determine necrosis or apoptosis.

The cells were seeded ($6.0x10^4$ cells per well in a 6-well plate) and cultured overnight. PI and Hoechst 33342 were prepared in PBS to serve as the staining solutions (0.5 $mg \cdot ml^{-1}$). The cells were treated with 20 μl staining solution in the dark and then incubated for 10 min at 37˚C. The cells were removed from the medium and fixed for 10 min with 2 ml cold methanol at 20-22˚C. After the removal of methanol, the cells were washed with PBS (1 ml) for 5 min, examined under a laser scanning confocal microscope (Zeiss LSM 880; Carl Zeiss AG), and photographed. The optical filters for excitation were 490-630 nm for PI and 350-460 nm for Hoechst. The ratio of red and blue fluorescence density was quantified by ZEN 2.3 (blue edition) software (Carl Zeiss Microscopy GmbH) and expressed as the percentage of PI-positive cells.

Annexin V/PI double staining. Annexin V and PI double staining is used to discriminate between apoptosis and necrosis; PI-positive staining reflects necrosis and Annexin V-positive/PI-negative staining reflects apoptosis (30). The cells were plated (6.0x104 cells per well) in a 6-well culture plate and then cultured overnight. The cells were then treated with 20 μM ASX for 24 h. The treated cells were then washed with ice-cold PBS and incubated with Annexin V-FITC and PI (FITC Annexin V Apoptosis Detection Kit; BD Pharmingen; BD Biosciences) in the dark according to the manufacturer's recommendations. The cells were fixed in 2% paraformaldehyde for 10 min at 20-22˚C, washed three times with 1 ml PBS for 5 min, and then examined under a laser scanning confocal microscope (Zeiss LSM 880; Carl Zeiss AG) and photographed.

Transfection of RIP1 siRNA. siGenome SMART pool siRNA for human RIP1 (5'-CCACUAGUCUGACGGAUAA-3, 5-UGAAUGACGUCAACGCAAA-3', 5'-GCACAAAUACGAACUUCAA-3' and 5'-GAUGAAAUCCAGUGACUUC-3') and the NC siRNA (siGenome None-Targeting siRNA Pool #1; 5'-UAGCGACUAAACACAUCAA, 5'-UAAGGCUAUGAAGAGAUAC-3', 5'-AUGUAUUGGCCUGUAUUAG-3' and 5'-AUGAACGUGAAUUGCUCAA-3') were obtained from GE Healthcare Dharmacon, Inc. Cells were transfected with 50 nmol RIP1 or NC siRNAs by using 1,2-dioleoyl-3-trimethylammonium-propane (DOTAP), following the manufacturer's instructions (Invitrogen; Thermo Fisher Scientific, Inc.), and then cultured for 24 h. Then, 24 h after transfection of RIP1 or NC siRNAs, the cells were treated with 20 μM ASX.

Measurement of LDH release. LDH release represents the permeabilization of the plasma membrane, a necrosis marker (31). LDH release was measured using an LDH assay kit (cat. no. ab102526; Abcam). Cell lysates were prepared using lysis buffer containing 0.1 M Tris (pH 7.4) and 10% Triton X-100. Cell lysates were centrifuged at 10,000 x g for 15 min at 4˚C. LDH activity in the culture medium and the cells was measured, as previously described (32). LDH release was quantified as a percentage of the total LDH content (LDH in the supernatant + LDH inside the cells).

Statistical analysis. All data are expressed as the mean ± standard error of the mean. All experiments were repeated three times. Number of each group was ten (n=10). The statistical differences among groups were evaluated by one-way analysis of variance (ANOVA) followed by Tukey's test. Statistical analysis was performed using SPSS 22.0 software (IBM Corp.). $P<0.05$ was considered to indicate a statistically significant difference.

Results

ASX increases ROS levels and decreases cell viability in AGS cells. To assess the appropriate culture time and concentration of ASX for ROS production in AGS cells, ROS levels were determined using different culture times and various concentrations of ASX. The cells were treated with ASX (20 μM) and cultured for 2 h. As shown in Fig. 1A, 20 μM ASX increased ROS levels in a time-dependent manner. Furthermore, ROS levels were highest at 2 h of culture. When the cells were treated with various concentrations (5, 10 and 20 μM) of ASX and cultured for 2 h, the highest level of ROS in AGS cells was obtained with 20 μM ASX (Fig. 1B). Thus, for further studies on ROS levels, cells were treated with 20 μM ASX for 2 h.

To determine whether ASX induces cell death and activates NADPH oxidase in normal cells, normal rat gastric epithelial RGM-1 cells were treated with 20 μM ASX for 2 h (for determination of NADPH oxidase activity) or different concentrations (5, 10 or 20 μM) of ASX for 24 h (for cell viability). ASX had no effect on cell viability or NADPH oxidase in RGM-1 cells (Fig. 1C and D). The results showed that ASX did not induce death of normal gastric epithelial cells.

ASX increases NADPH oxidase activity, which leads to cell death in AGS cells. To determine whether ASX-induced ROS production was linked to NADPH oxidase activation in AGS cells, the cells were pretreated with ML171, a specific inhibitor of NADPH oxidase 1, or an antioxidant, NAC, for 1 h, and then treated with ASX (20 μM) for 2 h. The ASX-induced increase in ROS levels was decreased by treatment with ML171 and NAC (Fig. 1E). As shown in Fig. 1F, ASX increased NADPH oxidase activity, which was reduced by ML171 in AGS cells. These results indicated that ASX induced NADPH oxidase activation, leading to increased ROS levels in AGS cells.

To examine whether ASX induces cell death, cell viability was assessed after 24 h of culture with various concentrations of ASX. ASX reduced cell viability in a dose-dependent manner (Fig. 2A).

Further, to determine whether NADPH oxidase and ROS induced ASX-associated cell death, the cells were pretreated with ML171 or NAC for 1 h followed by treatment with ASX for 24 h. As presented in Fig. 2B, both ML171 and NAC inhibited the ASX-induced decrease in cell viability.

To determine whether ML171 or NAC inhibited ASX-induced necrosis in AGS cells, PI and Hoechst 33342 double staining was performed (Fig. 2C). The density ratio of the red and blue fluorescence was quantified and expressed as PI-positive cells (%) (Fig. 2D). The number of necrotic AGS cells increased after ASX treatment, as indicated by the increase in the ratio of PI-positive cells. Both ML171 and NAC reduced the number of PI-positive cells, indicating that NAC

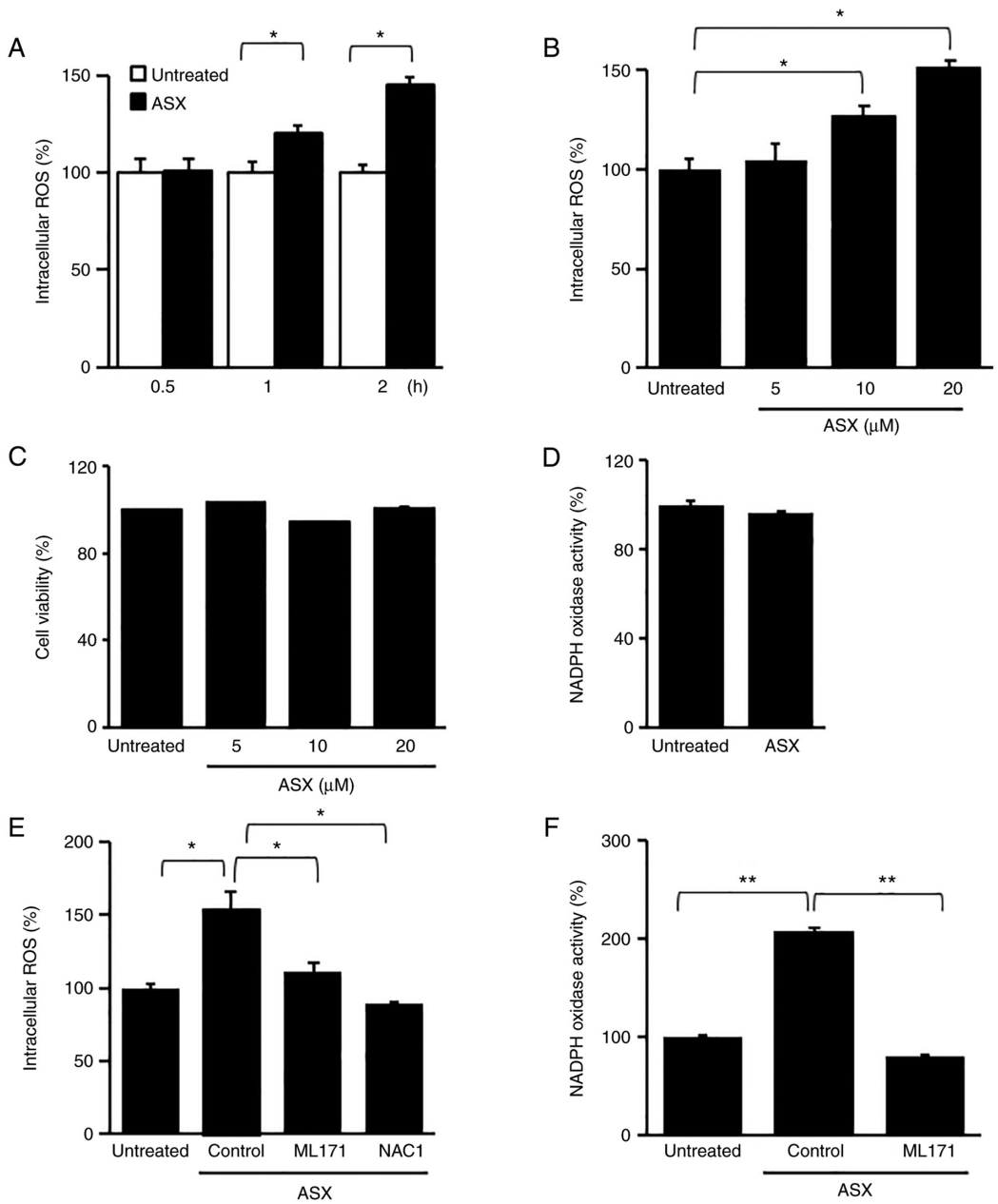

Figure 1. Levels of intracellular ROS, NADPH oxidase activity and cell viability in AGS cells or RGM-1 cells treated with ASX with or without ML171 or NAC. (A) Cells were treated with 20 μM ASX for the indicated time periods or (B) cells were treated with the indicated concentrations of ASX for 2 h and levels of intracellular ROS were analyzed using fluorescent DCF-DA. (C) RGM-1 cells were treated with the indicated concentrations of ASX for 24 h. The number of viable cells was determined using the trypan blue exclusion test. (D) RGM-1 cells were treated with 20 μM ASX for 2 h and NADPH oxidase activity in the membrane fraction was determined using a lucigenin assay. NADPH oxidase activity in cytosolic fraction was used as a negative control. (E) Cells were pretreated with 1 mM NAC or 2 μM ML171 for 1 h and then treated with 20 μM ASX for 2 h, and then levels of intracellular ROS were analyzed using fluorescent DCF-DA. (F) Cells were pretreated with 2 μM ML171 for 1 h and then treated with 20 μM ASX for 2 h, and then NADPH oxidase activity in the membrane fraction was determined using a lucigenin assay. NADPH oxidase activity in cytosolic fraction was used as a negative control. For ROS assays, the ROS level of cells that were not treated with ASX (untreated) was considered to be 100%. NADPH oxidase activity of cells that were not treated with ASX (untreated) was considered to be 100%. Data are presented as the mean ± standard error of the mean. *P<0.05 and **P<0.01 as determined by one-way ANOVA followed by Tukey's test. ROS, reactive oxygen species; ASX, astaxanthin; DCF-DA, dichlorofluorescein diacetate; NAC, N-acetyl cysteine.

and ML171 blocked ASX-induced necrotic cell death. These results suggested that ASX induced necrosis, which may be mediated by NADPH oxidase and increased ROS levels.

ASX activates necroptotic proteins in AGS cells. During necroptosis, the mRNA and protein levels of necroptotic proteins, including RIP1, RIP3 and MLKL, are upregulated (33,34). In the present study, ASX significantly increased the mRNA expression of RIP1 and RIP3 at 4 h compared with the untreated group. However, there were no significant changes in mRNA expression of MLKL by ASX treatment (Fig. 3A).

Total and phospho-specific forms of RIP1, RIP3 and MLKL were confirmed via western blotting to determine whether the effect of ASX on cell death involves necroptosis (Fig. 3B). It was found that ASX increased the protein expression of RIP1, RIP3 and MLKL. Moreover, ASX augmented the activation of RIP1, RIP3 and MLKL, as indicated by the increased levels of the phosphorylated forms of RIP1 and RIP3. These

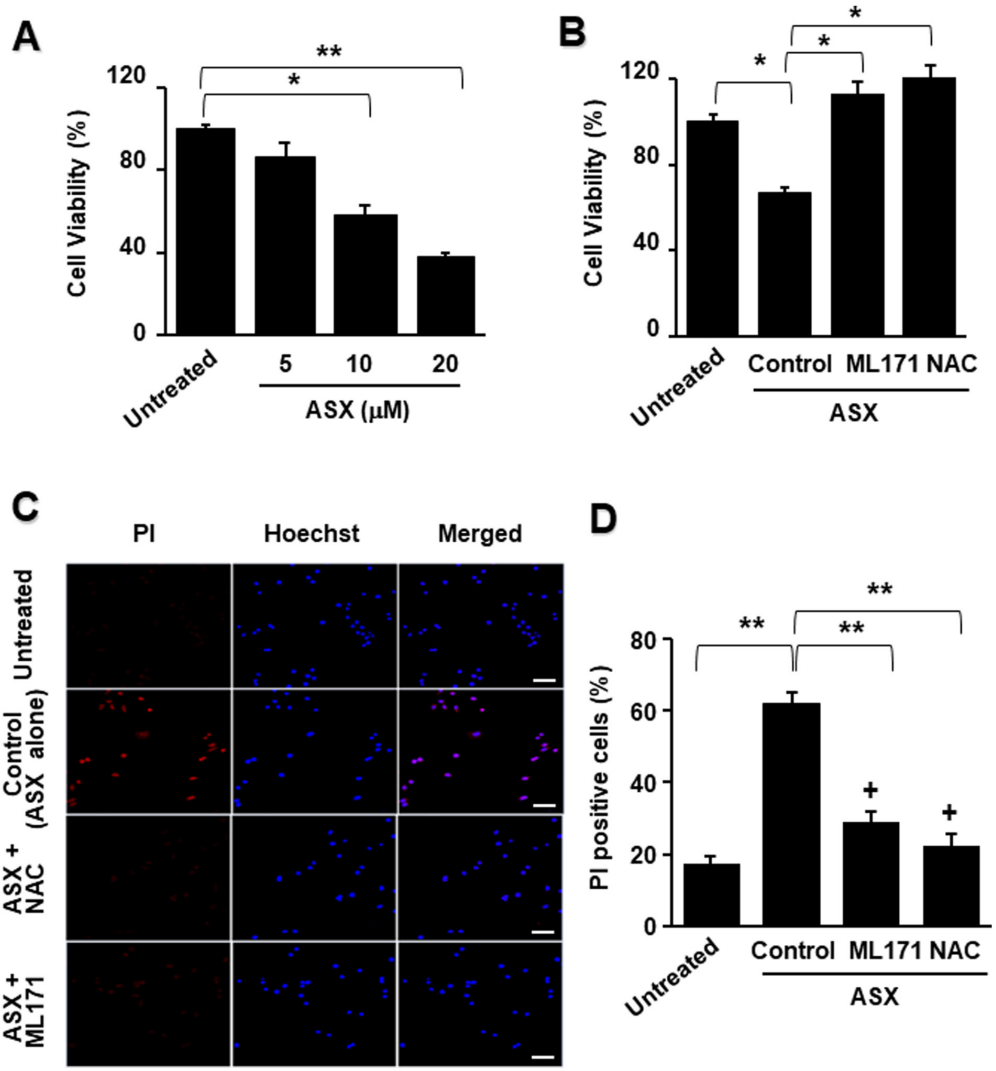

Figure 2. Cell viability and PI/Hoechst 33342 double staining of AGS cells treated with ASX with or without ML171 or NAC. (A) Cells were treated with the indicated concentrations of ASX for 24 h. (B-D) The cells were pretreated with 1 mM NAC or 2 μM ML171 for 1 h, and then treated with 20 μM ASX for 24 h. (A and B) The number of viable cells was determined using the trypan blue exclusion test. Viability of cells that were not treated with ASX (untreated) was set at 100%. (C) Cells were double stained with PI and Hoechst 33342. Nuclei were stained with Hoechst 33342 (blue). Scale bar, 50 μm. Dead cells resulting from necrosis are displayed in red, due to PI staining. Double staining of cells with Hoechst 33342 and PI distinguishes between cells with or without necrosis. (D) The ratio of red and blue fluorescence density was quantified and expressed as PI-positive cells (%). Data are presented as the mean ± standard error of the mean. *P<0.05 and **P<0.01 as determined by one-way ANOVA followed by Tukey's test. PI, propidium iodide; ASX, astaxanthin; NAC, N-acetyl cysteine.

results suggested the involvement of RIP1/RIP3/MLKL in ASX-induced necroptosis in AGS cells.

To further investigate the role of RIP1 in ASX-induced cell death, a gene silencing approach was used to specifically knock down RIP1. To confirm the inhibitory effect of RIP1 siRNA, the protein expression of RIP1 in AGS cells was measured after transfection with RIP1 or NC siRNA. The protein levels of RIP1 were notably suppressed in cells transfected with RIP1 siRNA compared with those transfected with the NC siRNA (Fig. 3C). ASX did not induce cell death in cells transfected with RIP1 siRNA, whereas ASX reduced the viability of cells transfected with the NC siRNA compared with the untreated group (Fig. 3D). These results indicated that ASX-induced cell death may occur through RIP1-mediated necroptosis.

ASX-induced cell death is suppressed by Nec-1, but not by z-VAD, in AGS cells. To determine whether ASX-induced cell death was necroptotic, the cells were treated with Nec-1 or z-VAD for 1 h prior to treatment with ASX for 24 h. Nec-1 is known to be a selective inhibitor of RIP1 (35). As shown in Fig. 4A and B, ASX-induced cell death and LDH release were inhibited by the necroptosis inhibitor Nec-1. A pan-caspase inhibitor, z-VAD, as an inhibitor of apoptosis, did not affect the ASX-induced increase in LDH release and cell death. These results suggested that ASX may induce necroptosis, but not apoptosis.

To determine whether ASX triggered necrotic cell death in AGS cells, PI and Hoechst 33342 double staining was performed (Fig. 4C). Hoechst 33342 is a bis-benzamide derivative that binds to AT-rich sequences in the minor groove of double-stranded DNA. Thus, this fluorescent stain is commonly used to visualize nuclei in microscopic studies (27). The plasma membrane-permeable dye PI can be detected in the necrotic cells. In the present study, Hoechst 33342 stained the nuclei of all cells, including healthy cells, producing blue fluorescence. However, live or apoptotic cells are impermeable

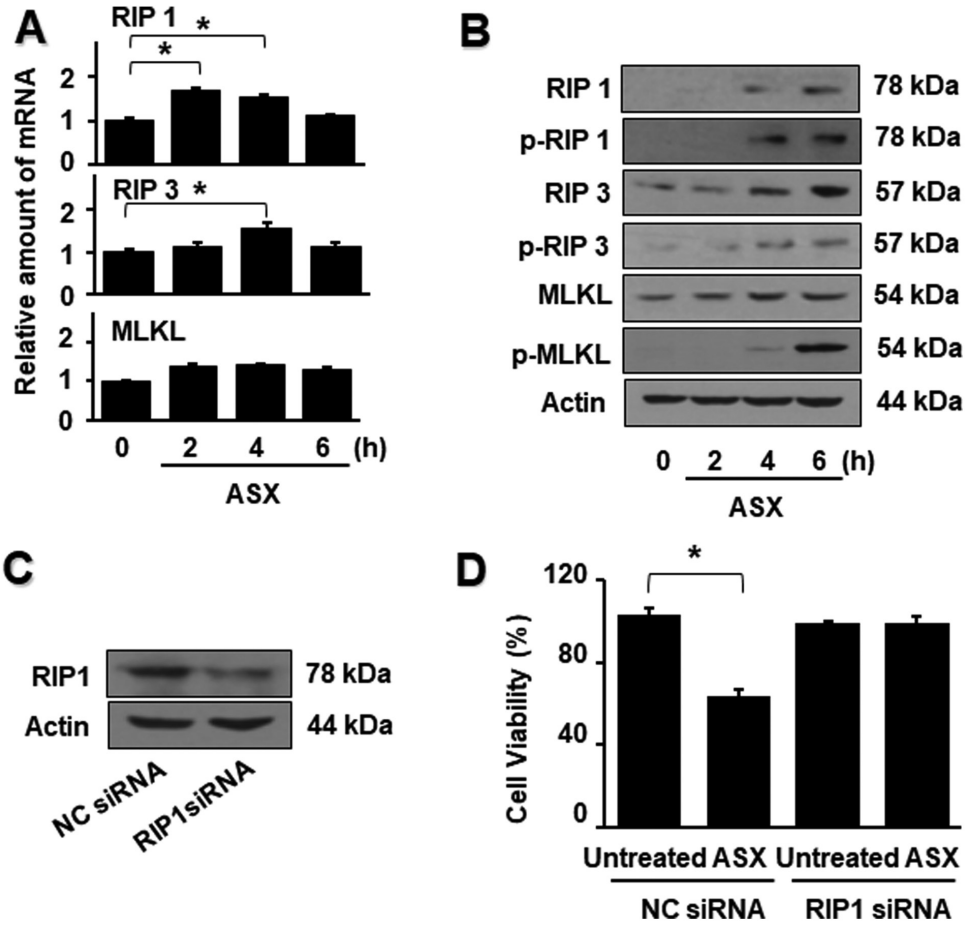

Figure 3. mRNA and protein expression levels of necroptosis-associated proteins in ASX-treated cells and cell viability of ASX-treated cells transfected with NC siRNA or RIP1 siRNA. (A and B) Cells were treated with 20 μM ASX for the indicated time periods. (A) mRNA expression levels of RIP1, RIP3 and MLKL were determined via reverse transcription-quantitative PCR analysis and normalized to those of β-actin. (B) The expression levels of p- and total forms of RIP1, RIP3 and MLKL were assessed via western blotting. Actin was used as the loading control. (C) Cells were transfected with siRNA (NC siRNA) or RIP1 siRNA for 24 h. The levels of RIP1 were assessed via western blotting. Actin served as a loading control. (D) Cells transfected with NC siRNA or RIP1 siRNA were treated with 20 μM ASX for 24 h. The number of viable cells was determined using the trypan blue exclusion test. The viability of cells that were not treated with ASX (untreated) was set at 100%. Data are presented as the mean ± standard error of the mean. *P<0.05 as determined by one-way ANOVA followed by Tukey's test. ASX, astaxanthin; RIP1, receptor-interacting protein kinase 1; NC, negative control; siRNA, small interfering RNA; MLKL, mixed lineage kinase domain-like protein; p-, phosphorylated.

to PI, which intensely stains necrotic cells red. As presented in Fig. 4C, AGS cells that underwent ASX treatment showed more necrotic cells, as determined by the increased ratio of PI-positive cells (Fig. 4D). Nec-1, a necroptosis inhibitor, decreased the number of PI-positive cells. However, z-VAD did not affect the ASX-induced increase in PI-positive cells, as determined by the ratio of red to blue fluorescence. These results showed that Nec-1 blocked ASX-induced necrotic cell death in AGS cells, suggesting that ASX may induce necroptosis in AGS cells.

ASX does not induce apoptosis in AGS cells. Caspase-9 activation amplifies the apoptosis cascade by activation of caspase-3 and other apoptosis mediators (36). Thus, the effect of ASX on caspase-9 activation in cells was determined. ASX did not increase the levels of active caspase-9 (Fig. 4E). As an index of apoptosis, the ratio of Bax/Bcl-2 was determined in cells treated with or without ASX (Fig. 4F). The Bax/Bcl-2 ratio was not affected by ASX. To determine whether ASX triggered apoptotic or necrotic cell death, double staining with Annexin V-FITC and PI was performed (Fig. 4G). Annexin V is a sensitive marker for detecting early apoptosis(30). Apoptotic cells can be distinguished from necrotic cells by double staining with PI. Annexin V-FITC and PI double staining easily distinguished apoptotic cells (shown as green fluorescence) from necrotic cells (shown as red fluorescence). ASX did not cause increased green fluorescence, but resulted in increased red fluorescence, indicating that ASX induced necrosis, but not apoptosis. Taken together, these results indicated that ASX-mediated cell death was related to necrosis/necroptosis.

Discussion

ASX shows anticancer effects by increasing or decreasing ROS levels, depending on the cell type, ASX concentration or redox state of the cancer cells. A number of studies have demonstrated that ASX serves as an antioxidant because it scavenges singlet oxygen and free radicals (37-39). However, a recent study showed that high-dose administration (5, 15 and 30 mg·kg^{-1} body weight) of ASX suppresses the activities of antioxidant enzymes (catalase and glutathione peroxidase) in the muscle tissues of mice (40).

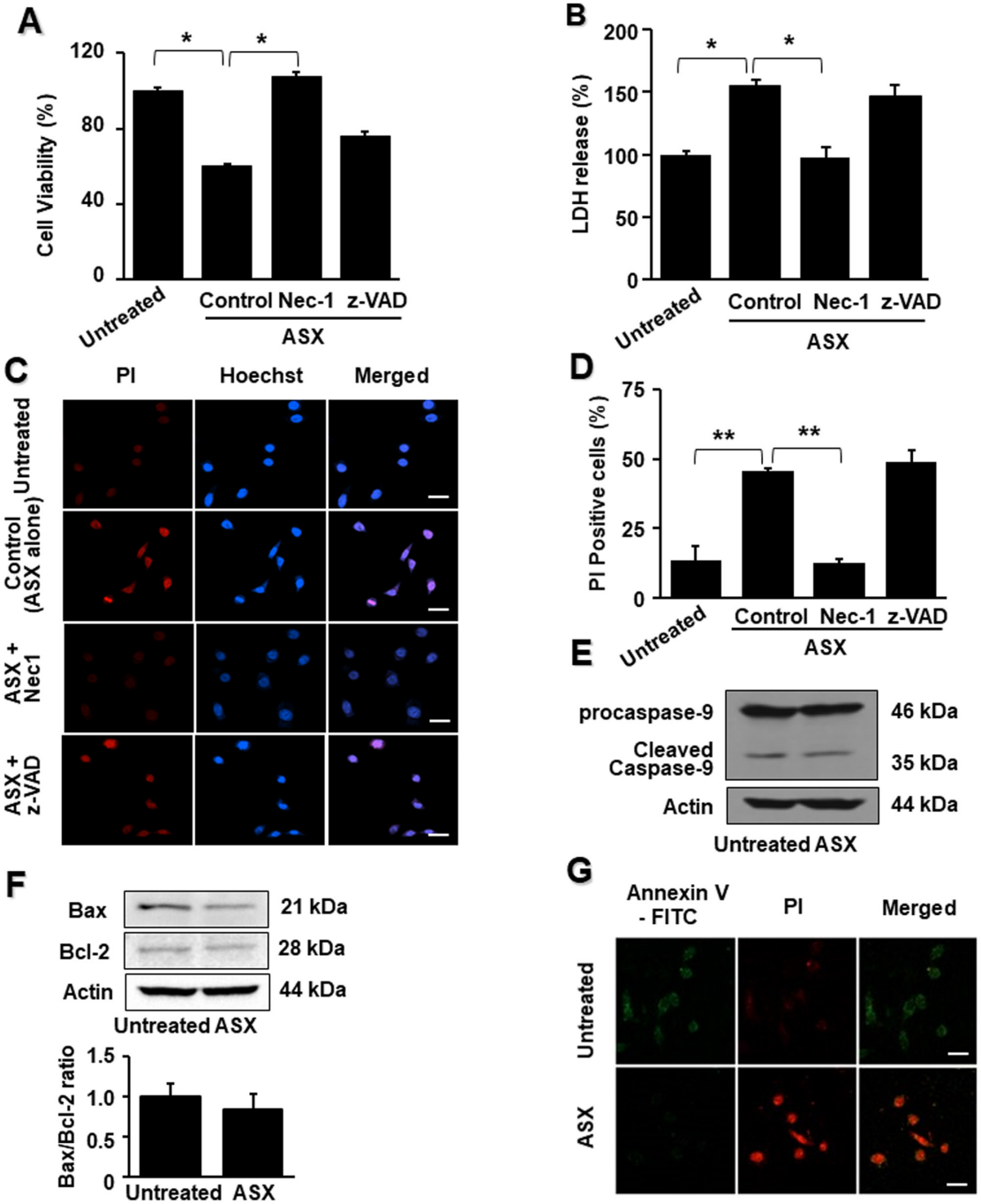

Figure 4. Cell viability, LDH release, PI/Hoechst 33342 double staining, cleavage of caspase-9, ratio of Bax/Bcl-2 and Annexin V-FITC/PI double staining of AGS cells treated with ASX with or without Nec-1 or z-VAD. (A-D) Cells were pretreated with 25 μM Nec-1 or 10 μM z-VAD for 1 h and then treated with 20 μM ASX for 24 h. (A) The number of viable cells was determined using the trypan blue exclusion test. (B) LDH activity was measured in the culture medium and cells. The LDH release was quantified as a percentage compared to the total LDH content (LDH in the supernatant+ LDH inside the cells). The value (cell viability or LDH release) of the cells that were not treated with ASX (untreated) was set at 100%. (C) Nuclei were stained with Hoechst 33342 (blue). Dead cells resulting from necrosis were displayed in red, due to PI staining. Double staining of cells with Hoechst 33342 and PI enabled us to distinguish between the typical features of necrosis. Scale bar, 20 μm. (D) The ratio of red and blue fluorescence density was quantified and expressed as PI-positive cells (%). (E-G) AGS cells were treated with 20 μM ASX for 24 h. (E) The expression levels of procaspase-9 and cleaved caspase-9 were assessed via western blotting. Actin served as a loading control. (F) Upper panel, levels of Bax, Bcl-2 and actin were assessed via western blotting. Lower panel, ratio of Bax/Bcl-2 was determined based on the protein band densities of Bax and Bcl-2. The ratio of Bax/Bcl-2 activity of cells that were not treated with ASX (untreated) was considered to be 1. (G) Fluorescence images of AGS cells were captured following Annexin V-FITC/PI double staining. Scale bar, 20 μm. Data are presented as the mean ± standard error of the mean. *P<0.05 and **P<0.01 as determined by one-way ANOVA followed by Tukey's test. LDH, lactate dehydrogenase; PI, propidium iodide; ASX, astaxanthin; Nec-1, Necrostatin-1.

As relatively few studies have determined the pro-oxidative activity of ASX, the mechanisms underlying it are not well defined. Previous research has shown that NADPH oxidase is a major source of ROS (41,42). The present study found that ASX increased NADPH oxidase, indicating that the source of ROS in ASX-treated cells is NADPH oxidase.

High levels of ROS mediate necroptotic cell death by increasing the phosphorylation of RIP1 and RIP3, which

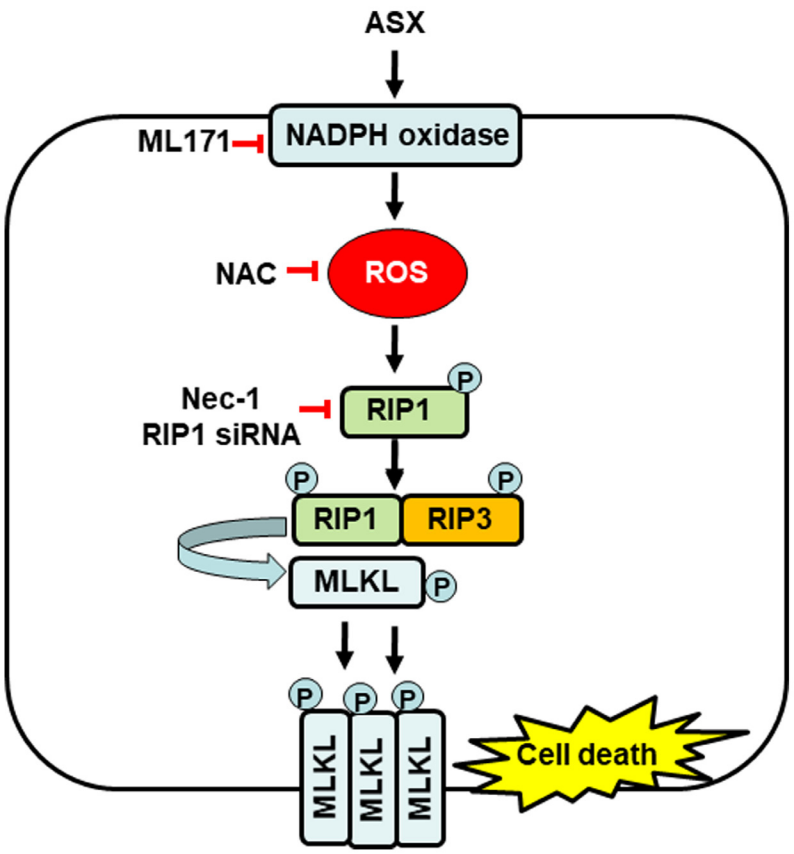

Figure 5. Proposed mechanism by which ASX induces necroptosis in gastric cancer AGS cells. High levels of ASX (20 μM) may activate NADPH oxidase and increase the production of ROS, which induce the phosphorylation of RIP1, thus, activating RIP3 and MLKL. Activated MLKL is translocated to the plasma membrane, where it possibly ruptures the cell membrane and causes necroptosis. Treatment with NADPH oxidase inhibitor ML171, antioxidant NAC and Nec-1, a specific inhibitor of RIP1, suppresses ASX-induced necroptosis in gastric cancer AGS cells. ASX, astaxanthin; ROS, reactive oxygen species; RIP, receptor-interacting protein kinase; MLKL, mixed lineage kinase domain-like protein; p-, phosphorylated; NAC, N-acetyl cysteine; Nec-1, Necrostatin-1; siRNA, small interfering RNA.

promotes necrosome formation (43-45). Regarding ROS and activation of RIP1/RIP3, RIP1 targets NADPH oxidase and increases ROS production in the plasma membrane in TNF-α-treated mouse fibroblasts (46). ROS increase the expression of RIP1 and RIP3 and their reciprocal binding (44,47) and stabilize this interaction in glioma cells stressed via photodynamic therapy (48). Therefore, ROS may regulate necroptosis by increasing RIP1 and RIP3 protein levels and their interactions. The current study showed that ASX-induced necroptosis was mediated via NADPH oxidase and ROS, as well as the activation of RIP1-RIP3, as Nec-1 (a specific inhibitor of RIP1), NAC (an antioxidant) and ML171 (an NADPH oxidase inhibitor) significantly suppressed the number of PI-positive AGS cells.

RIP3 binds to the plasma membrane and induces the phosphorylation of MLKL, which induces the oligomerization of p-MLKL to induce plasma membrane rupture and necroptosis (49). In the present study, MLKL was activated during ASX-induced necroptosis in AGS cells. The dead cells resulting from necrosis appeared red due to the PI staining. Hoechst 33342 and PI double staining allowed us to distinguish between the typical features of necrosis. Based on the PI and Hoechst 33342 staining results, ASX increased the number of PI-positive cells, which were inhibited by treatment with NAC, ML171 and Nec-1. However, z-VAD did not affect the ASX-induced increase in PI-positive cells. These results demonstrated that ASX-induced cell death occurred via necroptosis. Moreover, ASX did not induce caspase-9 activation. Moreover, in Annexin V/PI double staining, ASX did not increase the number of Annexin-positive cells, but increased the number of PI-positive cells at 24 h. These findings showed that ASX did not induce apoptosis, but did induce necrotic cell death.

In the present study, it was found that ASX induced an increase in NADPH oxidase activity, ROS production and phosphorylation of RIP1/RIP3/MLKL, leading to cell death in AGS cells. Treatment with the NADPH oxidase 1 inhibitor ML171 suppressed ASX-induced ROS production. High levels of ROS induce mitochondrial dysfunction and increase mitochondrial ROS levels (50,51). Moreover, treatment with ML171, antioxidant NAC and Nec-1, a specific inhibitor of RIP1, and transfection with RIP1 siRNA suppressed ASX-induced necroptosis. Therefore, it was concluded that NADPH oxidase is important in the production of ROS and, consequently, in ROS-mediated activation of RIP1-RIP3-MLK and necroptosis in gastric cancer AGS cells (Fig. 5).

Regarding the effect of ASX on normal cell viability, the current study did not find any effect on cell viability and NADPH oxidase activity in normal RGM-1 cells. Depending on their concentration and oxygen tension, carotenoids have been reported to act as antioxidants or pro-oxidants. The pro-oxidant activity of carotenoids is shown at increased

concentrations under high oxygen tension (52,53). Therefore, ASX-induced activation of NADPH oxidase and cell death may be affected by high concentrations of ASX and cellular environmental events in AGS cells.

For bioavailability of ASX in humans, 6 day-consumption of ASX (daily consumption of 250 g salmon; 5 μg ASX per gram of salmon flesh) results in plasma ASX concentrations of 39-52 nM (54). Furthermore, 12-week supplementation of 1 or 3 mg ASX (capsules containing ASX-rich oil) results in plasma concentrations of 18.9 and 62.4 nM, respectively, in Japanese middle-aged and senior subjects (55). Therefore, the concentration of ASX (20 μM) used in the present study is much higher than the concentration that results from dietary intake. These results suggested that a high concentration of ASX should be used to induce gastric cell necroptosis. Further studies should be performed to determine whether high concentrations of ASX induces necroptosis in various cancer cell lines *in vitro* and *in vivo*.

In the present study, AGS cells were used to determine the anticancer effects of ASX. The gastric adenocarcinoma AGS cell line is derived from untreated human adenocarcinoma of the stomach. The AGS cell line is a moderately differentiated human gastric adenocarcinoma hyperdiploid cell line. The AGS cell line has been shown to grow in athymic mice (56) and retain the same histochemical and cytological characteristics as the original malignant cells obtained from the patient (57). It is important to characterize human tumor cells *in vitro* in a detailed manner, as they serve as useful model systems for studies involving heterogeneous responses to anticancer drugs (57). Recently, this cell line has been widely used as a model system for evaluating cancer cell apoptosis (58-60).

AGS cells have more genetic changes and higher growth rates than normal cells (60,61). One example is tripartite motif containing 25 (TRIM25), a member of TRIM proteins that has been implicated in carcinogenesis. AGS cells show high expression of TRIM25, which contributes to higher growth rates compared with normal gastric epithelial cells (61). AGS cells exhibit abnormal expression of microRNA-372 (miR-372) (62). miR-372 maintains oncogene characteristics by targeting tumor necrosis factor-α-induced protein 1-regulated AGS cell growth (63). In a study by Guan *et al* (64) expression of the oncogene HER-2 in AGS cells was found to be twice that in normal gastric epithelial cells.

In addition, it is known that ROS are produced by several nutrients, such as vitamin C, zeaxanthin and β-carotene, which induce cell death in AGS cells (65-67). Therefore, in the present study, AGS cells were used to determine the anticancer mechanism of ASX.

In a study by Dong *et al* (68), Nec-1 and NADPH oxidase inhibitor diphenyleneiodonium prevent tumor necrosis factor-α, benzyloxycarbonyl-Val-Ala-Asp-fluoromethylketone and antimycin A (collectively termed TZA)-induced necroptosis by inhibiting the phosphorylation of RIP3 and MLKL in HK-2 cells. Recent studies have demonstrated that NAC suppresses necroptosis induced by high concentrations of iron or glucose through the inhibition of RIP1 phosphorylation (69,70). These studies suggest that NADPH oxidase-mediated ROS production may induce necroptosis through phosphorylation of RIP1, RIP3 and MLKL (69,70). Further studies are needed to determine whether treatment with ML171, NAC or Nec-1 suppresses ASX-induced expression and activation of RIP1, RIP3 and MLKL in AGS cells.

In conclusion, ASX increased intracellular ROS levels by activating NADPH oxidase, thereby, inducing necroptosis in gastric cancer AGS cells. NADPH oxidase-mediated ROS production may represent an underlying mechanism of ASX-induced necroptosis in gastric cancer AGS cells. Consequently, ASX could be used to treat gastric cancer based on its role in necroptotic signaling.

Acknowledgements

Not applicable.

Funding

This study was financially supported by a grant from the National Research Foundation of Korea, funded by the Korean Government (grant no. NRF-2021R1A2B5B02002353).

Availability of data and materials

All data generated or analyzed during this study are included in this published article.

Authors' contributions

HK conceived and designed the experiments. JWL assisted in designing the experiment. SK and HL performed the experiments. SK and JWL analyzed the data. JWL and HK confirm the authenticity of all raw data. SK wrote the paper. HK reviewed and edited the paper. All authors have read and approved the final manuscript.

Ethics approval and consent to participate

Not applicable.

Patient consent for publication

Not applicable.

Competing interests

The authors declare that they have no competing interests.

References

1. Yamashita E: Astaxanthin as a medical food. Funct Food Health Dis 3: 254-258, 2013.
2. Kidd P: Astaxanthin, cell membrane nutrient with diverse clinical benefits and anti-aging potential. Altern Med Rev 16: 355-364, 2011.
3. Zhang L and Wang H: Multiple mechanisms of anti-cancer effects exerted by astaxanthin. Mar Drugs 13: 4310-4330, 2015.
4. Fassett RG and Coombes JS: Astaxanthin: A potential therapeutic agent in cardiovascular disease. Mar Drugs 9: 447-465, 2011.
5. Li J, Dai W, Xia Y, Chen K, Li S, Liu T, Zhang R, Wang J, Lu W, Zhou Y, *et al*: Astaxanthin inhibits proliferation and induces apoptosis of human hepatocellular carcinoma cells via inhibition of NF-κB P65 and Wnt/B-catenin in vitro. Mar Drugs 13: 6064-6081, 2015.

6. Kim JH, Park JJ, Lee BJ, Joo MK, Chun HJ, Lee SW and Bak YT: Astaxanthin inhibits proliferation of human gastric cancer cell lines by interrupting cell cycle progression. Gut Liver 10: 369-374, 2016.
7. Hormozi M, Ghoreishi S and Baharvand P: Astaxanthin induces apoptosis and increases activity of antioxidant enzymes in LS-180 cells. Artif Cells Nanomed Biotechnol 47: 891-895, 2019.
8. Kochi T, Shimizu M, Sumi T, Kubota M, Shirakami Y, Tanaka T and Moriwaki H: Inhibitory effects of astaxanthin on azoxymethane-induced colonic preneoplastic lesions in C57/BL/KsJ-db/db mice. BMC Gastroenterol 14: 212, 2014.
9. Tanasawet S, Sukketsiri W, Chonpathompikunlert P, Klaypradit W, Sroyraya M and Hutamekalin P: Apoptotic effect of astaxanthin from white shrimp shells on lung cancer A549 cells. Trop J Pharm Res 19: 1835-1842, 2020.
10. Sowmya PR, Arathi BP, Vijay K, Baskaran V and Lakshminarayana R: Astaxanthin from shrimp efficiently modulates oxidative stress and allied cell death progression in MCF-7 cells treated synergistically with β-carotene and lutein from greens. Food Chem Toxicol 106: 58-69, 2017.
11. Chen D, Yu J and Zhang L: Necroptosis: An alternative cell death program defending against cancer. Biochim Biophys Acta 1865: 228-236, 2016.
12. Feng X, Song Q, Yu A, Tang H, Peng Z and Wang X: Receptor-interacting protein kinase 3 is a predictor of survival and plays a tumor suppressive role in colorectal cancer. Neoplasma 62: 592-601, 2015.
13. He S, Liang Y, Shao F and Wang X: Toll-like receptors activate programmed necrosis in macrophages through a receptor-interacting kinase-3-mediated pathway. Proc Natl Acad Sci USA 108: 20054-20059, 2011.
14. Ch'en IL, Tsau JS, Molkentin JD, Komatsu M and Hedrick SM: Mechanisms of necroptosis in T cells. J Exp Med 208: 633-641, 2011.
15. Lu JV, Chen HC and Walsh CM: Necroptotic signaling in adaptive and innate immunity. Semin Cell Dev Biol 35: 33-39, 2014.
16. Vanden Berghe T, Linkermann A, Jouan-Lanhouet S, Walczak H and Vandenabeele P: Regulated necrosis: The expanding network of non-apoptotic cell death pathways. Nat Rev Mol Cell Biol 15: 135-147, 2014.
17. Mifflin L, Ofengeim D and Yuan J: Receptor-interacting protein kinase 1 (RIPK1) as a therapeutic target. Nat Rev Drug Discov 19: 553-571, 2020.
18. Liu Y, Liu T, Lei T, Zhang D, Du S, Girani L, Qi D, Lin C, Tong R and Wang Y: RIP1/RIP3-regulated necroptosis as a target for multifaceted disease therapy (Review). Int J Mol Med 44: 771-786, 2019.
19. Lalaoui N and Brumatti G: Relevance of necroptosis in cancer. Immunol Cell Biol 95: 137-145, 2017.
20. Koo GB, Morgan MJ, Lee DG, Kim WJ, Yoon JH, Koo JS, Kim SI, Kim SJ, Son MK, Hong SS, *et al*: Methylation-dependent loss of RIP3 expression in cancer represses programmed necrosis in response to chemotherapeutics. Cell Res 25: 707-725, 2015.
21. Sun W, Yu W, Shen L and Huang T: MLKL is a potential prognostic marker in gastric cancer. Oncol Lett 18: 3830-3836, 2019.
22. Zhang Y, Su SS, Zhao S, Yang Z, Zhong CQ, Chen X, Cai Q, Yang ZH, Huang D, Wu R, *et al*: RIP1 autophosphorylation is promoted by mitochondrial ROS and is essential for RIP3 recruitment into necrosome. Nat Commun 8: 14329, 2017.
23. Moriwaki K and Chan FKM: RIP3: A molecular switch for necrosis and inflammation. Genes Dev 27: 1640-1649, 2013.
24. Skonieczna M, Hejmo T, Poterala-Hejmo A, Cieslar-Pobuda A and Buldak RJ: NADPH oxidases: Insights into selected functions and mechanisms of action in cancer and stem cells. Oxid Med Cell Longev 2017: 9420539, 2017.
25. Oparka M, Walczak J, Malinska D, van Oppen LM, Szczepanowska J, Koopman WJ and Wieckowski MR: Quantifying ROS levels using CM-H2DCFDA and HyPer. Methods 109: 3-11, 2016.
26. Livak KJ and Schmittgen TD: Analysis of relative gene expression data using real-time quantitative PCR and the 2(-Delta Delta C(T)) method. Methods 25: 402-408, 2001.
27. Lee J, Lim JW and Kim H: Lycopene inhibits oxidative stress-mdiated inflammatory responses in ethanol/palmitoleic acid-stimulatd pancreatic acinar AR42J cells. Int J Mol Sci 22: 2101, 2021.
28. Minkenberg I and Ferber E: Lucigenin-dependent chemiluminescence as a new assay for NAD(P)H-oxidase activity in particulate fractions of human polymorphonuclear leukocytes. J Immunol Methods 71: 61-67, 1984.
29. Crowley LC, Marfell BJ, and Waterhouse NJ: Analyzing cell death by nuclear staining with Hoechst 33342. Cold Spring Harb Protoc: Sep 1, 2016 (Epub ahead of print). doi: 10.1101/pdb.prot087205.
30. Sawai H and Domae N: Discrimination between primary necrosis and apoptosis by necrostatin-1 in Annexin V-positive/propidium iodide-negative cells. Biochem Biophys Res Commun 411: 569-573, 2011.
31. Chan FK-M, Moriwaki K and De Rosa MJ: Detection of necrosis by release of lactate dehydrogenase activity. Methods Mol Biol 979: 65-70, 2013.
32. López E, Figueroa S, Oset-Gasque MJ, and González MP: Apoptosis and necrosis: Two distinct events induced by cadmium in cortical neurons in culture. Br J Pharmacol 138: 901-911, 2003.
33. Zhu K, Liang W, Ma Z, Xu D, Cao S, Lu X, Liu N, Shan B, Qian L and Yuan J: Necroptosis promotes cell-autonomous activation of proinflammatory cytokine gene expression. Cell Death Dis 9: 500, 2018.
34. Yoon S, Kovalenko A, Bogdanov K and Wallach D: MLKL, the protein that mediates necroptosis, also regulates endosomal trafficking and extracellular vesicle generation. Immunity 47: 51-65.e7, 2017.
35. Christofferson DE, Li Y, Hitomi J, Zhou W, Upperman C, Zhu H, Gerber SA, Gygi S and Yuan J: A novel role for RIP1 kinase in mediating TNFα production. Cell Death Dis 3: e320, 2012.
36. McDonnell MA, Wang D, Khan SM, Vander Heiden MG and Kelekar A: Caspase-9 is activated in a cytochrome c-independent manner early during TNFalpha-induced apoptosis in murine cells. Cell Death Differ 10: 1005-1015, 2003.
37. Dose J, Matsugo S, Yokokawa H, Koshida Y, Okazaki S, Seidel U, Eggersdorfer M, Rimbach G and Esatbeyoglu T: Free radical scavenging and cellular antioxidant properties of astaxanthin. Int J Mol Sci 17: 103, 2016.
38. Kogure K: Novel Antioxidative activity of astaxanthin and its synergistic effect with vitamin E. J Nutr Sci Vitaminol (Tokyo) 65 (Suppl 1): S109-S112, 2019.
39. Landon R, Gueguen V, Petite H, Letourneur D, Pavon-Djavid G and Anagnostou F: Impact of astaxanthin on diabetes pathogenesis and chronic complications. Mar Drugs 18: 357, 2020.
40. Zhou Y, Baker JS, Chen X, Wang Y, Chen H, Davison GW and Yan X: High-dose astaxanthin supplementation suppresses antioxidant enzyme activity during moderate-intensity swimming training in mice. Nutrients 11: 1244, 2019.
41. Rastogi R, Geng X, Li F and Ding Y: NOX activation by subunit interaction and underlying mechanisms in disease. Front Cell Neurosci 10: 301, 2017.
42. Emanuele S, D'Anneo A, Calvaruso G, Cernigliaro C, Giuliano M and Lauricella M: The double-edged sword profile of redox signaling: Oxidative events as molecular switches in the balance between cell physiology and cancer. Chem Res Toxicol 31: 201-210, 2018.
43. Jia Y, Wang F, Guo Q, Li M, Wang L, Zhang Z, Jiang S, Jin H, Chen A, Tan S, *et al*: Curcumol induces RIPK1/RIPK3 complex-dependent necroptosis via JNK1/2-ROS signaling in hepatic stellate cells. Redox Biol 19: 375-387, 2018.
44. Zhang DW, Shao J, Lin J, Zhang N, Lu BJ, Lin SC, Dong MQ and Han J: RIP3, an energy metabolism regulator that switches TNF-induced cell death from apoptosis to necrosis. Science 325: 332-336, 2009.
45. Belizário J, Vieira-Cordeiro L and Enns S: Necroptotic cell death signaling and execution pathway: Lessons from knockout mice. Mediators Inflamm 2015: 128076, 2015.
46. Kim YS, Morgan MJ, Choksi S and Liu ZG: TNF-induced activation of the Nox1 NADPH oxidase and its role in the induction of necrotic cell death. Mol Cell 26: 675-687, 2007.
47. Cho YS, Challa S, Moquin D, Genga R, Ray TD, Guildford M and Chan FK: Phosphorylation-driven assembly of the RIP1-RIP3 complex regulates programmed necrosis and virus-induced inflammation. Cell 137: 1112-1123, 2009.
48. Lu B, Gong X, Wang ZQ, Ding Y, Wang C, Luo TF, Piao MH, Meng FK, Chi GF, Luo YN, *et al*: Shikonin induces glioma cell necroptosis in vitro by ROS overproduction and promoting RIP1/RIP3 necrosome formation. Acta Pharmacol Sin 38: 1543-1553, 2017.
49. Zhang Y, Chen X, Gueydan C and Han J: Plasma membrane changes during programmed cell deaths. Cell Res 28: 9-21, 2018.
50. Zorov DB, Juhaszova M and Sollott SJ: Mitochondrial reactive oxygen species (ROS) and ROS-induced ROS release. Physiol Rev 94: 909-950, 2014.
51. Peoples JN, Saraf A, Ghazal N, Pham TT and Kwong JQ: Mitochondrial dysfunction and oxidative stress in heart disease. Exp Mol Med 51: 1-13, 2019.

52. Tapiero H, Townsend DM and Tew KD: The role of carotenoids in the prevention of human pathologies. Biomed Pharmacother 58: 100-110, 2004.
53. Shin J, Song MH, Oh JW, Keum YS and Saini RK: Pro-oxidant actions of carotenoids in triggering apoptosis of cancer cells: A review of emerging evidence. Antioxidants 9: 532, 2020.
54. Rüfer CE, Moeseneder J, Briviba K, Rechkemmer G and Bub A: Bioavailability of astaxanthin stereoisomers from wild (*Oncorhynchus* spp.) and aquacultured (*Salmo salar*) salmon in healthy men: A randomised, double-blind study. Br J Nutr 99: 1048-1054, 2008.
55. Miyazawa T, Nakagawa K, Kimura F, Satoh A and Miyazawa T: Plasma carotenoid concentrations before and after supplementation with astaxanthin in middle-aged and senior subjects. Biosci Biotechnol Biochem 75: 1856-1858, 2011.
56. Barati T, Haddadi M, Sadeghi F, Muhammadnejad S, Muhammadnejad A, Heidarian R, Arjomandnejad M and Amanpour S: AGS cell line xenograft tumor as a suitable gastric adenocarcinoma model: Growth kinetic characterization and immunohistochemistry analysis. Iran J Basic Med Sci 21: 678-681, 2018.
57. Barranco SC, Townsend CM Jr, Casartelli C, Macik BG, Burger NL, Boerwinkle WR and Gourley WK: Establishment and characterization of an in vitro model system for human adenocarcinoma of the stomach. Cancer Res 43: 1703-1709, 1983.
58. Park HS, Hong NR, Ahn TS, Kim H, Jung MH and Kim BJ: Apoptosis of AGS human gastric adenocarcinoma cells by methanolic extract of Dictamnus. Pharmacogn Mag 11 (Suppl 2): S329-S336, 2015.
59. Tsai CL, Chiu YM, Ho TY, Hsieh CT, Shieh DC, Lee YJ, Tsay GJ and Wu YY: Gallic Acid induces apoptosis in human gastric adenocarcinoma cells. Anticancer Res 38: 2057-2067, 2018.
60. Ngabire D, Seong YA, Patil MP, Niyonizigiye I, Seo YB and Kim GD: Induction of apoptosis and G1 phase cell cycle arrest by Aster incisus in AGS gastric adenocarcinoma cells. Int J Oncol 53: 2300-2308, 2018.
61. Zhu Z, Wang Y, Zhang C, Yu S, Zhu Q, Hou K and Yan B: TRIM25 blockade by RNA interference inhibited migration and invasion of gastric cancer cells through TGF-β signaling. Sci Rep 6: 19070, 2016.
62. Li X, Zhang X, Liu X, Tan Z, Yang C, Ding X, Hu X, Zhou J, Xiang S, Zhou C, *et al*: Caudatin induces cell apoptosis in gastric cancer cells through modulation of Wnt/β-catenin signaling. Oncol Rep 30: 677-684, 2013.
63. Zhou C, Li X, Zhang X, Liu X, Tan Z, Yang C and Zhang J: microRNA-372 maintains oncogene characteristics by targeting TNFAIP1 and affects NFκB signaling in human gastric carcinoma cells. Int J Oncol 42: 635-642, 2013.
64. Guan SS, Chang J, Cheng CC, Luo TY, Ho AS, Wang CC, Wu CT and Liu SH: Afatinib and its encapsulated polymeric micelles inhibits HER2-overexpressed colorectal tumor cell growth in vitro and in vivo. Oncotarget 5: 4868-4880, 2014.
65. Lim JY, Kim D, Kim BR, Jun JS, Yeom JS, Park JS, Seo JH, Park CH, Woo HO, Youn HS, *et al*: Vitamin C induces apoptosis in AGS cells via production of ROS of mitochondria. Oncol Lett 12: 4270-4276, 2016.
66. Sheng YN, Luo YH, Liu SB, Xu WT, Zhang Y, Zhang T, Xue H, Zuo WB, Li YN, Wang CY, *et al*: Zeaxanthin induces apoptosis via ROS-regulated MAPK and AKT signaling pathway in human gastric cancer cells. OncoTargets Ther 13: 10995-11006, 2020.
67. Park Y, Choi J, Lim JW and Kim H: β-Carotene-induced apoptosis is mediated with loss of Ku proteins in gastric cancer AGS cells. Genes Nutr 10: 467, 2015.
68. Dong W, Li Z, Chen Y, Zhang L, Ye Z, Liang H, Li R, Xu L, Zhang B, Liu S, *et al*: NADPH oxidase inhibitor, diphenyleneiodonium prevents necroptosis in HK-2 cells. Biomed Rep 7: 226-230, 2017.
69. Tian Q, Qin B, Gu Y, Zhou L, Chen S, Zhang S, Zhang S, Han Q, Liu Y and Wu X: ROS-mediated necroptosis is involved in iron overload-induced osteoblastic cell death. Oxid Med Cell Longev 2020: 1295382, 2020.
70. Deragon MA, McCaig WD, Patel PS, Haluska RJ, Hodges AL, Sosunov SA, Murphy MP, Ten VS and LaRocca TJ: Mitochondrial ROS prime the hyperglycemic shift from apoptosis to necroptosis. Cell Death Discov 6: 132, 2020.